The *in vivo* performance of plasmonic nanobubbles as cell theranostic agents in zebrafish hosting prostate cancer xenografts

Daniel S. Wagner[1], **Nikki A. Delk**[1], **Ekaterina Y. Lukianova-Hleb**[2], **Jason H. Hafner**[3], **Mary C. Farach-Carson**[1], and **Dmitri O. Lapotko**[2,3,1]

[1]Department of Biochemistry&Cell Biology, Rice University, Houston, TX, 77251-1892, USA

[2]Joint American-Belarussian Laboratory for Fundamental and Biomedical Nanophotonics, A. V. Lykov Heat & Mass Transfer Institute, Minsk, 220072, Belarus

[3]Department of Physics & Astronomy, Rice University, Houston, TX, 77005, USA

Abstract

Cell theranostics is a new approach that unites diagnosis, therapy and confirmation (guidance) of the results of therapy in one single process at cell level, thus principally improving both the rapidity and precision of treatment. The ideal theranostic agent will support all three of the above functions *in vivo* with cellular resolution, allowing individual assessment of disease state and the elimination of diseased cells while leaving healthy cells intact. We have developed and evaluated plasmonic nanobubbles (PNBs) as an *in vivo* tunable theranostic cellular agent in zebrafish hosting prostate cancer xenografts. PNBs were selectively generated around gold nanoparticles in cancer cells in the zebrafish with short single laser pulses. By varying the energy of the laser pulse, we dynamically tuned the PNB size in a theranostic sequence of two PNBs: an initial small PNB detected a cancer cell through optical scattering, followed by a second bigger PNB, which mechanically ablated this cell without damage to surrounding tissue, while its optical scattering confirmed the destruction of the cell. Thus PNBs supported the diagnosis and guided ablation of individual human cancer cells in a living organism without damage to the host.

Keywords

theranostics; cell; plasmonic nanobubble; gold nanoparticle; laser; cancer

1. Introduction

The separation of diagnosis, therapy and confirmation of the results of therapy (therapy guidance) is an inherent challenge in medical practice that slows down treatment and lowers its accuracy. Theranostics is a new approach [1–4] that unites these three stages in one single process, thus principally improving both the rapidity and precision of treatment.

[1]Rice University, Physics and Astronomy - MS 61, 6100 Main Street, Houston, TX 77005, Tel.: 713-348-3708, Fax.: 713-348-4150, dl5@rice.edu.

However, the limited sensitivity of many methods that cannot specifically access diseased cells while leaving healthy cell intact, also compromises their accuracy and prevents early-stage diagnosis and treatment. The ideal theranostic agent will support multiple tunable functions at the cellular level for imaging and guided treatment. No existing agent can provide this tunability of diagnostic, ablative and guidance functions as a single particle and within a single cell. While great strides have been made in the development of a fluorescent probe [3,5,6], various capsule type carriers [7,8], nanoparticles [5–9], including plasmonic nanoparticles [3,10–12] and vapor bubbles [13–15], most of these probes have specific pre-set functions that cannot be tuned dynamically in disease-specific cells. Many of these probes use methods that still rely primarily on macro- rather than nano- processes. This disadvantage limits the accuracy and safety of their medical applications.

We hypothesize that by combining the diagnosis-specific targeting and photothermal properties of plasmonic (gold) nanoparticles (NP) with the mechanical and optical properties of transient vapor nanobubbles we can produce a tunable nanoscale theranostic agent. This agent is not an NP but an NP-generated on demand event (Fig. 1a,b), a plasmonic nanobubble (PNB). A PNB emerges when a plasmonic gold NP is locally overheated with a short laser pulse. As a result the NP evaporates a very thin volume (nanometer size) of the surrounding medium, thus creating a vapor nanobubble that expands and then collapses within nanoseconds. Its fast expansion produces a localized mechanical impact. In addition, the bubble scatters the light, thus acting as an optical probe. We have defined this bubble as a plasmonic nanobubble because a plasmonic NP acts as its source and determines its energy and location [16].

Plasmonic gold NPs alone have been extensively studied as cellular agents due to their relative safety [17] compared to any other nanoparticles. Gold NPs strongly absorb and scatter light at visible and near infrared wavelengths due to localized surface plasmon resonance [18–20]. The strong absorption, scattering, and electromagnetic field enhancement caused by this effect enabled optical diagnostic [11,21–23] and therapeutic [11,12,22,24] potential. However, background scattering by cells and tissues often dominates the NP scattering signal, resulting in low sensitivity and specificity of NP-based diagnostic methods. Therapeutic NP technologies employ photothermal effects such as hyperthermia [11,22,24] and pressure or shock waves [25]. However, these are macro-rather than nano-scale effects, that cannot be localized and precisely controlled within single specific cells. Hyperthermia treatment requires a relatively long time (minutes), and due to the inevitable thermal diffusion such treatment cannot be localized better than in a millimeter range. Consequently gold NP hypothermia can damage healthy cells and tissues. The high cellular loads of nanoparticles (10^{3-7} NP/cell) required to support the effect, low selectivity and tunability, together with the challenges of NP delivery, pose significant limitations to combining accurate diagnosis and targeted therapy at cell level.

Recently we have suggested using plasmonic nanobubbles instead of gold NPs for diagnostic and therapeutic applications. We have shown that PNB generation *in vitro* is dependant on the energy of the laser pulse and, therefore, can be tuned [26]. We have shown that small sublethal bubbles or lethal large bubble can be generated predictably with specific excitation energies in tissue culture cells [27]. We have shown that specific antibodies to cell surface receptors can direct the uptake of NPs and that the clustering of NPs through receptor mediated endocytosis can increase the sensitivity of PNB generation [26,28]. We have also demonstrated the unique optical properties of PNBs that turned out to be much brighter than gold NPs [29,30] Our *in vitro* and cell culture experiments have shown that PNBs are a potentially powerful theranostic agent. The successful clinical development of new materials and technologies requires their *in vivo* validation. Due to the large size of most experimental models and the variable optical qualities of different tissues, transitioning

from *in vitro* methods to *in vivo* is challenging for many nanotechnologies and nanomaterials. To support this transition of PNB theranostics we have combined the properties of PNBs as cancer cell agents [27] with the discovered properties of a small optically transparent *in vivo* model, the zebrafish embryo, in particular, its ability to tolerate and support the remote and non-invasive generation and detection of PNBs [31]. In this work we have tested the potential of PNB theranostics *in vivo* and we have generated, tuned and detected PNBs in human prostate cancer xenografts transplanted into zebrafish embryo hosts (Fig. 1a). Cultured metastatic human prostate cancer cells C4-2B were labeled with 60 nm gold nanoparticles conjugated with C225 anti-EGFR antibodies (EGF receptor is over-expressed by these tumors) and DiI fluorescent dye to provide a label for viability and lineage tracing after transplantation (Fig. 1c). We have found that single human prostate cancer cells can be detected and ablated under optical guidance *in vivo* by tunable PNBs in a single theranostic procedure.

2. Materials and methods

2.1. Optical generation and detection of plasmonic nanobubbles

A plasmonic nanobubble (PNB) (Fig. 2) emerges when a plasmonic gold NP is locally overheated with a short laser pulse. As a result the NP evaporates a very thin volume (nanometer size) of the surrounding medium, thus creating a vapor nanobubble that expands and then collapses within a short nanosecond. The fast expansion of the vapor bubble has a localized mechanical and non-thermal impact on the environment [27,32,33]. In addition, the bubble scatters the light, thus acting as an optical probe [27,29,30,32,33]. We have defined this bubble as a PNB because its energy is provided by a plasmonic nanoparticle, and its point of effort is determined by the location of a gold NP. Optical generation and detection of the PNB was performed with our own previously developed photothermal laser microscope [32]. Imaging of the cells and nanobubbles was realized in two simultaneous modes: time-resolved imaging and time-response.

For time resolved imaging we have used side-scattering of the short optical pulse (690 nm). Pixel image amplitude in the center of such a spot was measured as I_{sc}. To quantify optical contrast of the PNB relative to that of the *cell or tissue* alone we have analyzed optical contrast K_{amp}:

$$K_{amp} = (I_{sc}(t) - I_{bc})/(I_{sc}(0) - I_{bc1}),$$

where *t* is the delay time of the probe pulse relative to the pump pulse (10 ns) and zero time corresponds to the scattering by an intact *object* alone (tissue or cell) prior to its exposure to a pump pulse, I_{bc} and I_{bc1} are the background pixel amplitudes. Thus K_{amp} characterizes the sensitivity and specificity of the PNB as an optical probe.

While allowing the determination of the location and contrast of the PNB, the pulsed imaging cannot provide kinetic measurement. The latter was realized in a time-response mode. PNBs were shown to produce very specific signals that allow the measurement of the bubble lifetime that characterizes a maximal diameter of the bubble [32,33]. Image and response modes were used simultaneously to combine the measurement of optical and mechanical properties of PNBs.

Bright-field imaging has been realized with the same experimental set up by using a standard microscope unit and the above mentioned camera. Fluorescence of DiI was activated with a continuous laser beam at 532 nm that has been directed into a sample. Thus we have obtained and quantified four independent optical signals *in vitro* and *in vivo*: bright

field image (characterized morphological structure of the object), fluorescent image (was used to detect the cells and to monitor their integrity), scattering time-resolved image (was used to detect the and to compare its brightness to that of the tissue and cells) and scattering time response (was used to characterize the size of PNB).

2.2. Nanoparticles

Conjugates of gold spheres 60 nm with anti-epidermal growth factor receptor (EGFR) antibody C225 were fabricated using covalent conjugation by Nanopartz Inc. (Salt Lake City, UT). NP conjugates were fabricated with surface chemistry that prevented their spontaneous aggregation in physiological media. The plasmon resonance wavelength of such gold nanoparticles (NP) is very close to 532 nm, as has been verified with optical spectroscopy of the NP suspension. Gold NPs of 60 nm size are known to be biologically safe [17,34]. However, we have monitored their cytotoxicity after incubating the cells with NPs and, in addition, have monitored the viability of the embryos after transplantation of the NP-targeted cells into zebrafish embryos. We have not found cytotoxic effects. The embryos with gold NPs have survived the cell transplantation. Therefore, we concluded that the employed gold NP conjugates were safe.

2.3. Cells

C4-2B prostate cancer (PC) cells were obtained from the American Type Culture Collection and maintained as described by Gurski *et al.* [35]. For nanoparticle treatment, cells were seeded in 6-well tissue culture dishes (Corning) and grown to 60% confluency. When the cells were ready for treatment, T-medium was removed and the cells were washed once with 1X phosphate buffered saline (PBS, Gibco/Invitrogen). The cells then were fed serum free RPMI Medium 1640 (Gibco/Invitrogen) containing C225-conjugated nanoparticles (NP) at a concentration of 5 µl NP: 1 ml media and incubated with the NP-containing media for 30 minutes in the $37°C$ CO_2 growth chamber. Control cells were fed serum free RPMI Medium 1640 without nanoparticles. Following incubation, the cells were washed to remove free nanoparticles, trypsinized, washed gently once in 1X PBS, repelleted, and finally suspended in serum free RPMI Medium 1640. Cell viability was checked using trypan blue staining. Individual cells were exposed to the laser pulses for the PNB generation. We have studied 25–30 cells for each sample. Coupling of NP-C225 conjugates to cellular membrane and their internalization has been verified with SEM (Fig. 3a, b).

2.4. Zebrafish

To establish the xenograft model [36,37], cells from the human prostate metastatic cell line, C4-2B, were transplanted into blastula stage zebrafish embryos. We labeled the C4-2B cells with gold nanoparticles prior to transplantation to isolate variables associated with the *in vivo* delivery of nanoparticles. The C4-2B cells were incubated with C225 (anti EGFR) conjugated 60 nm gold nanoparticles. Conjugation to C225 directs uptake of gold nanoparticles through the endocytic pathway, which promotes the clusterization of gold nanoparticles [28,38]. The cells were washed, trypsinized and labeled with Vybrant DiI CM (Invitrogen) for cell tracking by fluorescent microscopy. C4-2B cells were introduced into blastula stage embryos using a standard cell transplantation methodology. Embryos were cultured at $28°C$ for one hour of recovery and then transferred to a $35°C$ incubator. Two days post fertilization, embryos were sorted for efficient engraftment of the C4-2B cells. Engrafted embryos were anesthetized in Tricaine and mounted in 1.5% low melt agarose for observation and PNB generation. Following imaging and PNB generation assays embryos were removed from the low melt agarose and cultured at $35°C$ for an additional three days.

3. Results

3.1. Theranostic action of tunable plasmonic nanobubbles in individual cells

Firstly, we tested PNB generation in individual C4-2B cancer cells *in vitro* loaded with C225 conjugated 60nm gold nanoparticles. Individual cells were exposed to a single laser pulse at 532 nm, 0.5 ns (Fig. 4a). The PNBs were detected simultaneously with time-resolved side-scattering images (that revealed PNB brightness and location, Fig. 4h,i) and the time-responses (that have delivered the PNB lifetime as a measure of its maximal diameter, Fig. 4k,l). The smallest PNBs (10 ns lifetime) were detected in individual cells at the threshold laser fluence of 45 mJ/cm^2. PNB lifetime increased with the fluence to 72 ns (Fig. 4k, Table 1) and PNBs became 15 times brighter than the cell (Fig. 4h, Table 1), and much brighter than gold NPs (whose scattering was weaker than the cellular scattering (Fig. 4g). No visible signs of morphological disruption of the cell (Fig. 4b) or change in DiI fluorescence (Fig. 4e) were detected after the 1st PNB generated at 125 mJ/cm^2. Previously we had found that the cells were damaged by PNBs with a lifetime above 110 ns, while shorter (smaller) PNBs did not compromise short-term viability of the cells [27,32]. Therefore, we concluded that cells survived the first PNB that acted as a diagnostic probe. Further increase of the laser fluence of the follow-up second pulse to 175 mJ/cm^2 produced in the same cell a 2nd PNB with increased brightness and lifetime relative to the first PNB (Fig. 4i,l, Table 1).

Within 20–30 s after the second PNB, the cell fluorescence dimmed (Fig. 4f), and the cell appeared disrupted (Fig. 4c versus Fig. 4a and 4b). Therefore, the second, larger PNB destroyed the cell since the vital fluorescent dye apparently leaked out of the cell and the visual appearance of the cell changed significantly. Optical contrast and the lifetime of this ablative PNB increased by more than three times compared to those of the first PNB (Table 1) and allowed guidance of the ablative action. The change of the PNB function in the cell was rapidly achieved by increasing the fluence of the laser pulse. Identical laser treatment of the collateral cells incubated only with DiI (without NPs) returned no PNBs (Table 1) with the scattering signals similar to those shown at Fig. 4g,j. We have never observed any signs of damage in collateral cells providing that the PNB has been generated only in one target cell. This has demonstrated a single cell selectivity of the PNB action.

In addition, we have monitored cell state with a scanning electron microscope (Leo Supra 55 VP scanning electron microscope, Zeiss NTS GmbH, Jena, Germany). Fig. 3a,b shows the cell after the incubation with gold NPs. Gold NPs were initially accumulated at the cellular membrane (Fig. 3a) and eventually were internalized due to receptor-mediated endocytosis (Fig. 3b). The cells were exposed to laser pulses with parallel monitoring of the PNBs and their lifetime (size). Cells were fixed with glutaraldehyde immediately after the exposure to laser pulses (within 1 min). Fig. 3c and 3d show the cells after the exposure to a single pump laser pulse that resulted in the PNB with 25±5 ns lifetime (the 1st PNB) and 300±42 ns lifetime (ablative, the 2nd PNB), respectively. While the first PNB did not change the cell structure (Fig. 3c versus 3b), the second, bigger PNB had a dramatic effect on the size, shape and structure of the cell (Fig. 3d versus 3c and 3b). Such changes assume the mechanical damage of the membrane and presumably the cytoskeleton. The cell damage has also been clearly confirmed with the change of fluorescence from the vital label following the generation of the PNB. This *in vitro* model has allowed us to determine the PNB selectivity and their tunability in individual cells.

3.2. PNB theranostics *in vivo*

Transitioning from the *in vitro* cell culture assays to *in vivo* systems is challenging and was considered the main goal of this work. We have developed a novel *in vivo* model by using

zebrafish. The zebrafish is a vertebrate organism that is relatively optically transparent, develops quite fast and is physiologically similar to humans. The zebrafish has already been evaluated for analysis of the distribution and toxicity of plasmonic (gold) NPs [39–41] and has also allowed efficient optical manipulations including laser microsurgery and sensing [42–46]. These findings allowed us to consider zebrafish embryos for plasmonic nanomedicine (optical scattering diagnosis, photothermal diagnosis and therapy, ultrasound and optical methods for drug delivery, cell manipulation and surgery). Furthermore, the zebrafish is a model for diverse cancers [47–52], which are promising targets for plasmonic therapies. Therefore, the zebrafish has an excellent potential for nanophotonic medicine. To test the applicability of PNB generation *in vivo*, we transplanted the fluorescent-labeled prostate cancer C4-2B cells into zebrafish embryos. Two days after transplantation, PC cells were distributed throughout the embryos with concentrations in the cardinal vessels and large numbers of single cells in the ventral tail veins (Fig. 1c). Three conditions (NP+ and NP− xenografts and ungrafted negative controls) were scanned with the laser pulses under identical fluence of the laser pulse. The embryos were imaged using bright field (Fig. 1a,5a–c), fluorescence (Fig. 1c,5d–f) and optical scattering (Fig. 5g–i). Using fluorescent imaging, we positioned the embryo so that each cancer cell matched the center of a laser beam (Fig. 5d) because cancer cells cannot be distinguished from host tissue in the bright field (Fig. 5a) and scattering images (Fig. 5g). We have scanned up to 20 cancer cells in each embryo. Each cancer cell was exposed to a single pump laser pulse #1 at a fluence of 125 mJ/cm^2 (Fig. 1a). We observed PNB-specific time response (Fig. 5k) and bright spot-shaped scattering images (Fig. 5h) only in the locations of the cancer cells. No PNBs were detected in non-fluorescent areas of the embryo including large heme rich blood vessels which can make PNBs under high fluence [31]. Thus we concluded that the PNBs were selectively generated only in cancer cells and not in surrounding normal host cells. The optical contrast of the first PNBs was found to be about one order of magnitude higher than that of the tissue scattering (Fig. 5g,h, Table 1), and its lifetime was comparable to that obtained previously for cultured cells (Table 1, Fig. 5k). The first PNB did not alter the bright field and fluorescent images (Fig. 5b,e) but was bright enough to detect a single cancer cell in a tissue.

Then the same area of the embryo was rapidly irradiated with a second pulse with a fluence of 175 mJ/cm^2 (Fig. 1b). The second PNBs were brighter and had higher contrast (Fig. 5i, Table 1) with a five fold longer lifetime relative to the first PNB (Table 1, Fig. 5l). Within 20 s after the second PNB, we observed a loss of DiI fluorescence (Fig. 5f) and concluded the cell was destroyed. However, we observed no changes in the bright field (Fig. 5c) and scattering images of this area, indicating that the damage was limited to the target cell. Therefore, sequential PNB generation in a single cell demonstrated the three stages of theranostics: detection of a cancer cell with the first PNB, ablation of the detected cell with the second PNB, and real time optical guidance of the cell destruction through optical parameters of the second PNB.

The identical laser treatment of the control embryos containing C4-2B cells without NPs returned no PNBs at the fluence level of 175 mJ/cm^2 returned no PNBs in both cancer and embryonic cells (Table 1). Therefore, we concluded that the PNBs were generated specifically in NP-containing individual cancer cells. The PNB-treated embryos with cancer cells were observed for up to seven days after PNB generation and all of them survived the PNBs.

4. Discussion

Unlike other vapor bubbles (generated with heat, ultrasound and optical breakdown [13–15,53]), the PNB thermally insulates the outer environment from the high temperature of a heated NP [27,32,33], thus reducing the risk of thermal damage to a minimum. The

mechanical and optical properties of the bubble are determined by its maximal diameter (Fig. 1a,b). This in turn depends upon optical energy being absorbed and converted into heat by the plasmonic NP. For these reasons, PNB properties can be precisely varied or tuned with the energy of a laser pulse (from 100 nm to tens of micrometers). Since the generation of a PNB occurs at the location of the NP, specific targeting of NPs will provide a very specific and localized effect of PNBs.

We have extrapolated the published data for vapor bubbles [14,54] and used the measured lifetime of PNBs to estimate their maximal diameters: the PNBs with 60–70 ns lifetime were estimated to be 500-1000 nm, while PNBs with a lifetime of 300 ns were estimated with 2500–5000 nm diameter. The latter is close to the size of the cell (10–14 µm), a feature that explains the ablative effect. The cell ablation was an immediate mechanical, not thermal phenomenon, because we did not detect any elevation of the temperature in time-responses after the collapse of the PNB: the signal returned to its baseline thus indicating an ambient temperature (Fig. 4l, 5l). Mechanical damage has also been confirmed with SEM images (Fig. 3).

PNB specificity is essential for biomedical applications. One mechanism for improving specificity is to have cancer cells convert the NPs into a more efficient PNB catalyst by the uptake of NPs through endocytosis and formation of clusters of NPs in the endocytotic pathway. The PNB thresholds and lifetimes we observed for the single identical NPs and their clusters (studied separately in water, Table 1) indicated that the PNBs observed in the cells and in the embryos were generated around NP clusters, not around single NPs. As we have shown previously, the clusterization of NPs lowered the PNB threshold [32,33], thus increasing the specificity of PNB generation compared to that of any known antibody-based targeting: under the specific level of laser fluence only the cells with NP clusters produced PNBs, while cells with single, non-specifically coupled NPs did not.

The reported cell level theranostics *in vivo* suggests several avenues for the further development and application of PNB technologies (Table 2). The PNB as a dynamically tunable probe may have research, clinical, biological and bioengineering applications. The PNB theranostic method offers a flexible rapid platform for developing treatments for many pathological conditions at cellular level. The rapid response of the PNB is compatible with the automatic real-time adjustment of PNB impact and function. Furthermore, the technology is compatible with established surgical and diagnostic optical technologies (optical catheters and probes) for localized delivery and detection of optical radiation in tissues. Given this flexibility and the use of non-toxic nanoparticles, we predict that this technology can be rapidly translated to the clinic for a variety of applications.

Conclusions

Our experiments have demonstrated that the PNB is a new, on demand and tunable cellular agent that supports diagnosis and guided treatment and is able to unite them in one rapid procedure at cell level. This tunable agent provided detection and selective guided ablation of individual metastatic prostate cancer cells *in vivo* during a single theranostic procedure and without damage to the host organism. Being focused on the first experimental observation of the theranostic effect of a tunable agent (PNB) *in vivo*, future work will address several important issues: *in vivo* targeting of gold nanoparticles, toxic effect associated with ablation of a tumor of significant size, and the delivery and collection of optical radiation in deep tissue. All these factors are beyond the scope of this article, however, they are all the subject of our ongoing and future work. Our immediate goal was to obtain proof of the concept of cell theranostics *in vivo* with a dynamically tunable agent, the plasmonic nanobubble.

Acknowledgments

References

1. McCarthy JR. The future of theranostic nanoagents. Nanomedicine 2009;4:693–695. [PubMed: 19839803]

2. Hartman KB, Wilson LJ, Rosenblum MG. Detecting and treating cancer with nanotechnology. Mol Diagn Ther 2008;12:1–14. [PubMed: 18288878]

3. Prigodich AE, Seferos DS, Massich MD, Giljohann DA, Lane BC, Mirkin CA. Nano-flares for mRNA regulation and detection. ACS Nano 2009;3:2147–2152. [PubMed: 19702321]

4. Picard FJ, Bergeron MG. Rapid molecular theranostics in infectious diseases. Drug Discov Today 2002;7:1092–1101. [PubMed: 12546841]

5. Al-Jamal WT, Al-Jamal KT, Tian B, Cakebread A, Halket JM, Kostarelos K. Tumor targeting of functionalized quantum dot-liposome hybrids by intravenous administration. Mol Pharm 2009;6:520–530. [PubMed: 19718803]

6. Santra S, Kaittanis C, Grimm J, Perez JM. Drug/dye-loaded, multifunctional iron oxide nanoparticles for combined targeted cancer therapy and dual optical/magnetic resonance imaging. Small 2009;5:1862–1868. [PubMed: 19384879]

7. Torchilin VP. Targeted pharmaceutical nanocarriers for cancer therapy and imaging. AAPS J 2007;9:E128–E147. [PubMed: 17614355]

8. Gullotti E, Yeo Y. Extracellularly activated nanocarriers: a new paradigm of tumor targeted drug delivery. Mol Pharm 2009;6:1041–1051. [PubMed: 19366234]

9. Sajja HK, East MP, Mao H, Wang YA, Nie S, Yang L. Development of multifunctional nanoparticles for targeted drug delivery and noninvasive imaging of therapeutic effect. Curr Drug Discov Technol 2009;6:43–51. [PubMed: 19275541]

10. El-Sayed IH, Huang X, El-Sayed MA. Surface plasmon resonance scattering and absorption of anti-EGFR antibody conjugated gold nanoparticles in cancer diagnostics: applications in oral cancer. Nano Lett 2005;5:829–834. [PubMed: 15884879]

11. Loo C, Lowery A, Halas N, West J, Drezek R. Immunotargeted nanoshells for integrated cancer imaging and therapy. Nano Lett 2005;5:709–711. [PubMed: 15826113]

12. Pitsillides CM, Joe EK, Wei X, Anderson RR, Lin CP. Selective cell targeting with light-absorbing microparticles and nanoparticles. Biophys J 2003;84:4023–4032. [PubMed: 12770906]

13. Postema M, van Wamel A, Lancee C, de Jong N. Ultrasound-induced encapsulated microbubble phenomena. Ultrasound Med Biol 2004;30:827–840. [PubMed: 15219962]

14. Vogel A, Noack J, Hüttmann G, Paltauf G. Mechanisms of femtosecond laser nanosurgery of cells and tissues. Appl Phys B 2005;81:1015–1047.

15. Prentice P, Cuschieri A, Dholakia K, Prausnitz M, Campbell P. Membrane disruption by optically controlled microbubble cavitation. Nat Phys 2005;1:107–110.

16. Lukianova-Hleb EY, Hu Y, Latterini L, Tarpani L, Lee S, Drezek RA, et al. Plasmonic nanobubbles as transient vapor nanobubbles generated around plasmonic nanoparticles. ACS Nano 2010;4:2109–2123. [PubMed: 20307085]

17. Lewinski N, Colvin V, Drezek R. Cytotoxicity of nanoparticles. Small 2008;4:26–49. [PubMed: 18165959]

18. Jun Y-W, Sheikholeslami S, Hostetter DR, Tajon C, Craik CS, Alivisatos AP. Continuous imaging of plasmon rulers in live cells reveals early-stage caspase-3 activation at the single-molecule level. Proc Natl Acad Sci U S A 2009;106:17735–17740. [PubMed: 19805121]

19. Zhang J, Fu Y, Liang D, Nowaczyk K, Zhao RY, Lackowicz JR. Single-cell fluorescence imaging using metal plasmon-coupled probe 2: single molecule counting on lifetime imaging. Nano Lett 2008;8:1179–1186. [PubMed: 18341300]

20. Alkilany AM, Nagaria P, Hexel CR, Shaw TJ, Murphy CJ, Wyatt MD. Cellular uptake and cytotoxicity of gold nanorods: molecular origin of cytotoxicity and surface effects. Small 2009;5:701–708. [PubMed: 19226599]

21. Kumar S, Harrison N, Richards-Kortum R, Sokolov K. Plasmonic nanoparticles with affinity and delivery functionalities for imaging intracellular biomarkers in live cells: actin in cultured fibroblasts. Nano Lett 2007;7:1338–1343. [PubMed: 17439187]

22. Huang X, El-Sayed I, Qian W, El-Sayed M. Cancer cell imaging and photothermal therapy in the near-infrared region by using gold nanorods. J Am Chem Soc 2006;128:2115–2120. [PubMed: 16464114]

23. Walter NG, Huang C-Y, Manzo AJ, Sobhy MA. Do-it-yourself guide: How to use the modern single-molecule toolkit. Nat Methods 2008;5:475–489. [PubMed: 18511916]

24. Tong L, Zhao Y, Huff TB, Hansen MN, Wei A, Cheng J-X. Gold nanorods mediate tumor cell death by compromising membrane integrity. Adv Mater 2007;19:3136–3141. [PubMed: 19020672]

25. Lee S, Anderson T, Zhang H, Flotte TJ, Doukas AG. Alteration of cell membrane by stress waves in vitro. Ultrasound Med Biol 1996;22:1285–1293. [PubMed: 9123654]

26. Hleb EY, Hafner JH, Myers JN, Hanna EY, Rostro BC, Zhdanok SA, et al. LANTCET: elimination of solid tumor cells with photothermal bubbles generated around clusters of gold nanoparticles. Nanomedicine 2008;3:647–667. [PubMed: 18817468]

27. Lukianova-Hleb EY, Hanna E, Hafner JH, Lapotko DO. Tunable plasmonic nanobubbles for cell theranostics. Nanotechnology 2010;21:085102.

28. Lapotko D, Lukianova-Hleb E, Oraevsky A. Clusterization of nanoparticles during their interaction with living cells. Nanomedicine 2007;2:241–253. [PubMed: 17716124]

29. Hleb E, Lapotko D. Influence of transient environmental photothermal effects on optical scattering by gold nanoparticles. Nano Lett 2009;9:2160–2166. [PubMed: 19374436]

30. Hleb EY, Hu Y, Drezek RA, Hafner JH, Lapotko DO. Photothermal bubbles as optical scattering probes for imaging living cells. Nanomedicine 2008;3:797–812. [PubMed: 19025454]

31. Lukianova-Hleb E, Santiago C, Wagner D, Hafner J, Lapotko D. Generation and detection of plasmonic nanobubbles in zebrafish. Nanotechnology 2010;21:225102. [PubMed: 20453288]

32. Lapotko D. Plasmonic nanoparticle-generated photothermal bubbles and their biomedical applications. Nanomedicine 2009;7:813–845. [PubMed: 19839816]

33. Lapotko D. Optical excitation and detection of vapor bubbles around plasmonic nanoparticles. Opt Express 2009;17:2538–2556. [PubMed: 19219157]

34. Oberdorster G, Oberdorster E, Oberdorster J. Nanotoxicology: an emerging discipline evolving from studies of ultrafine particles. Environ Health Perspect 2005;113:823–839. [PubMed: 16002369]

35. Gurski LA, Jha AK, Zhang C, Jia X, Farach-Carson MC. Hyaluronic acid-based hydrogels as 3D matrices for in vitro evaluation of chemotherapeutic drugs using poorly adherent prostate cancer cells. Biomaterials 2009;30:6076–6085. [PubMed: 19695694]

36. Amatruda JF, Patton EE. Genetic models of cancer in zebrafish. Int Rev Cell Mol Biol 2008;271:1–34. [PubMed: 19081540]

37. Goessling W, North TE, Zon LI. New waves of discovery: modeling cancer in zebrafish. J Clin Oncol 2007;25:2473–2479. [PubMed: 17557959]

38. Chan WCW, Chithrani BD. Elucidating the mechanism of cellular uptake and removal of proteincoated gold nanoparticles of different sizes and shapes. Nano Lett 2007;7:1542–1550. [PubMed: 17465586]

39. Browning LM, Lee KJ, Huang T, Nallathamby PD, Lowman JE, Xu X-HN. Random walk of single gold nanoparticles in zebrafish embryos leading to stochastic toxic effects on embryonic developments. Nanoscale 2009;1:138–152. [PubMed: 20644873]

40. Griffitt RJ, Hyndman K, Denslow ND, Barber D. Comparison of molecular and histological changes in zebrafish gills exposed to metallic nanoparticles. Toxicol Sci 2009;107:404–415. [PubMed: 19073994]

41. Bar-Ilan O, Albrecht RM, Fako VE, Furgeson DY. Toxicity assessments of multisized gold and silver nanoparticles in zebrafish embryos. Small 2009;5:1897–1910. [PubMed: 19437466]

42. Sakakura M, Kajiyama S, Tsutsumi M, Si J, Fukusaki E, Tamaru Y, et al. Femtosecond pulsed laser as a microscalpel for microdissection and isolation of specific sections from biological samples. Japan J Appl Physics 2007;46 5859–586.

43. Kohli V, Elezzabi AY. Laser surgery of zebrafish (Danio rerio) embryos using femtosecond laser pulses: Optimal parameters for exogenous material delivery, and the laser's effect on short- and long-term development. BMC Biotechnol 2008;8:7. [PubMed: 18230185]

44. Jorgensen A, Nielsen JE, Morthorst JE, Bjerregaard P, Leffers H. Laser capture microdissection of gonads from juvenile zebrafish. Reprod Biol Endocrinol 2009;7:97. [PubMed: 19747405]

45. Liu KS, Fetcho JR. Laser ablations reveal functional relationships of segmental hindbrain neurons in zebrafish. Neuron 1990;23:325–335. [PubMed: 10399938]

46. Halloran MC, Sato-Maeda M, Warren JT Jr, Su F, Lele Z, Krone PH, et al. Laser-induced gene expression in specific cells of transgenic zebrafish. Development 2000;127:1953–1960. [PubMed: 10751183]

47. Langenau DM, Traver D, Ferrando AA, Kutok JL, Aster JC, Kanki JP, et al. Myc-induced T cell leukemia in transgenic zebrafish. Science 2003;299:887–890. [PubMed: 12574629]

48. Mizgireuv IV, Revskoy SY. Transplantable tumor lines generated in clonal zebrafish. Cancer Res 2006;66:3120–3125. [PubMed: 16540662]

49. Nicol S, Ribatti D, Cotelli F, Presta M. Mammalian tumor xenografts induce neovascularization in zebrafish embryos. Cancer Res 2007;67:2927–2931. [PubMed: 17409396]

50. Nicoli S, Presta M. The zebrafish/tumor xenograft angiogenesis assay. Nat Protoc 2007;2:2918–2923. [PubMed: 18007628]

51. White RM, Sessa A, Burke C, Bowman T, LeBlanc J, Ceol C, et al. Transparent adult zebrafish as a tool for in vivo transplantation analysis. Cell Stem Cell 2008;2:183–189. [PubMed: 18371439]

52. Amatruda JF, Shepard JL, Stern HM, Zon LI. Zebrafish as a cancer model system. Cancer Cell 2002;1:229–231. [PubMed: 12086858]

53. Coussio CC, Farny CH, Haar GT, Roy RA. Role of acoustic cavitation in the delivery and monitoring of cancer treatment by high-intensity focused ultrasound (HIFU). Int J Hyperthermia 2007;23:105–120. [PubMed: 17578336]

54. Hutson S, Ma X. Plasma and cavitation dynamics during pulsed laser microsurgery in vivo. Phys Rev Lett 2007;99:158104. [PubMed: 17995217]
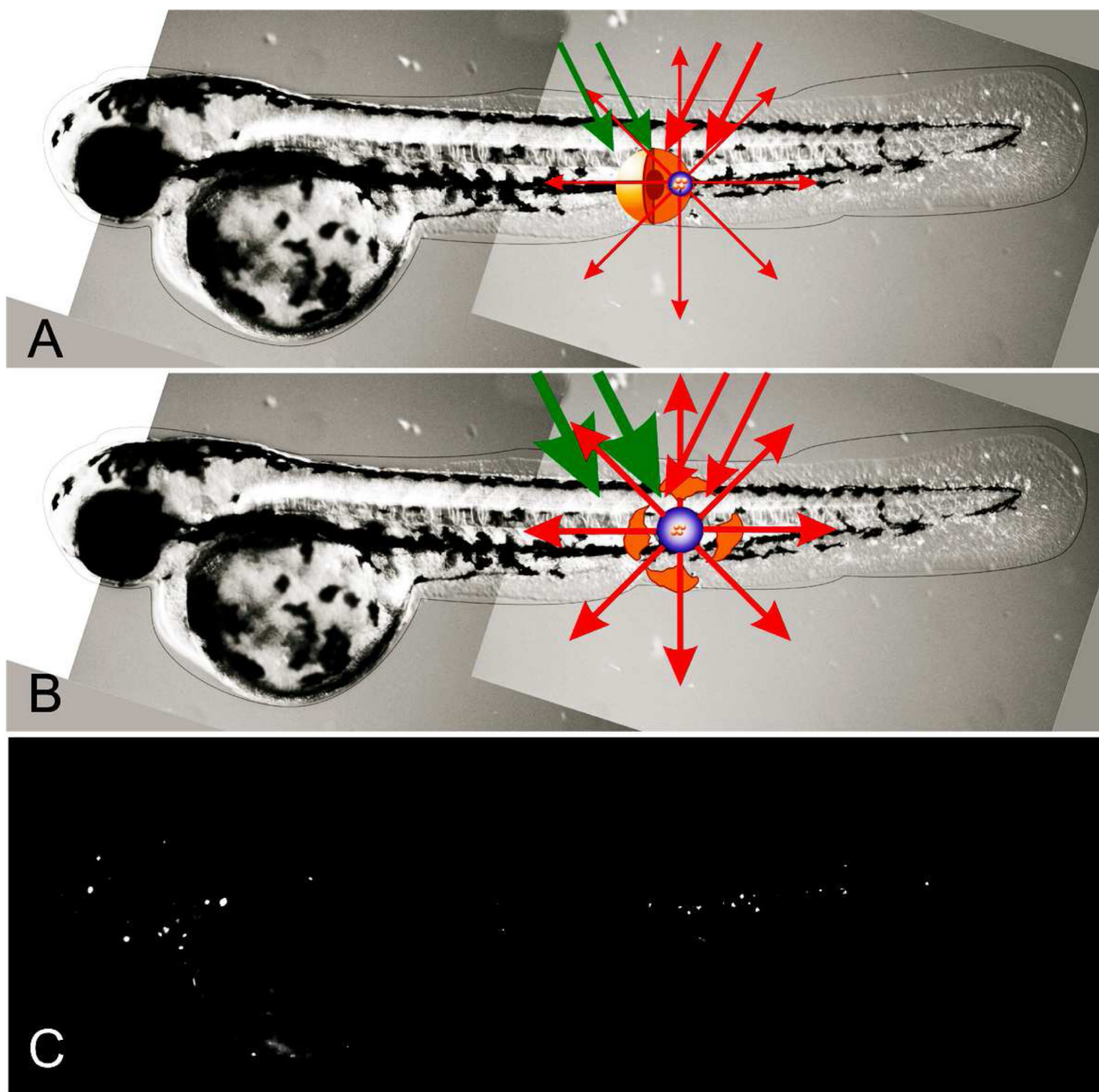
Figure 1.
PNB theranostics *in vivo* includes the generation and detection of the two sequential PNBs: (a) small PNB is generated (with green pump laser pulse) in zebrafish and in specific cell and detected (with red probe laser pulse) thus sensing the cell; (b) the next bigger PNB (generated with the second pulse of higher energy) destroys the cell, while optical scattering of the 2nd PNB guides the destruction; (c) fluorescent image of the embryo shows prostate labeled cancer cells scattered through its body.
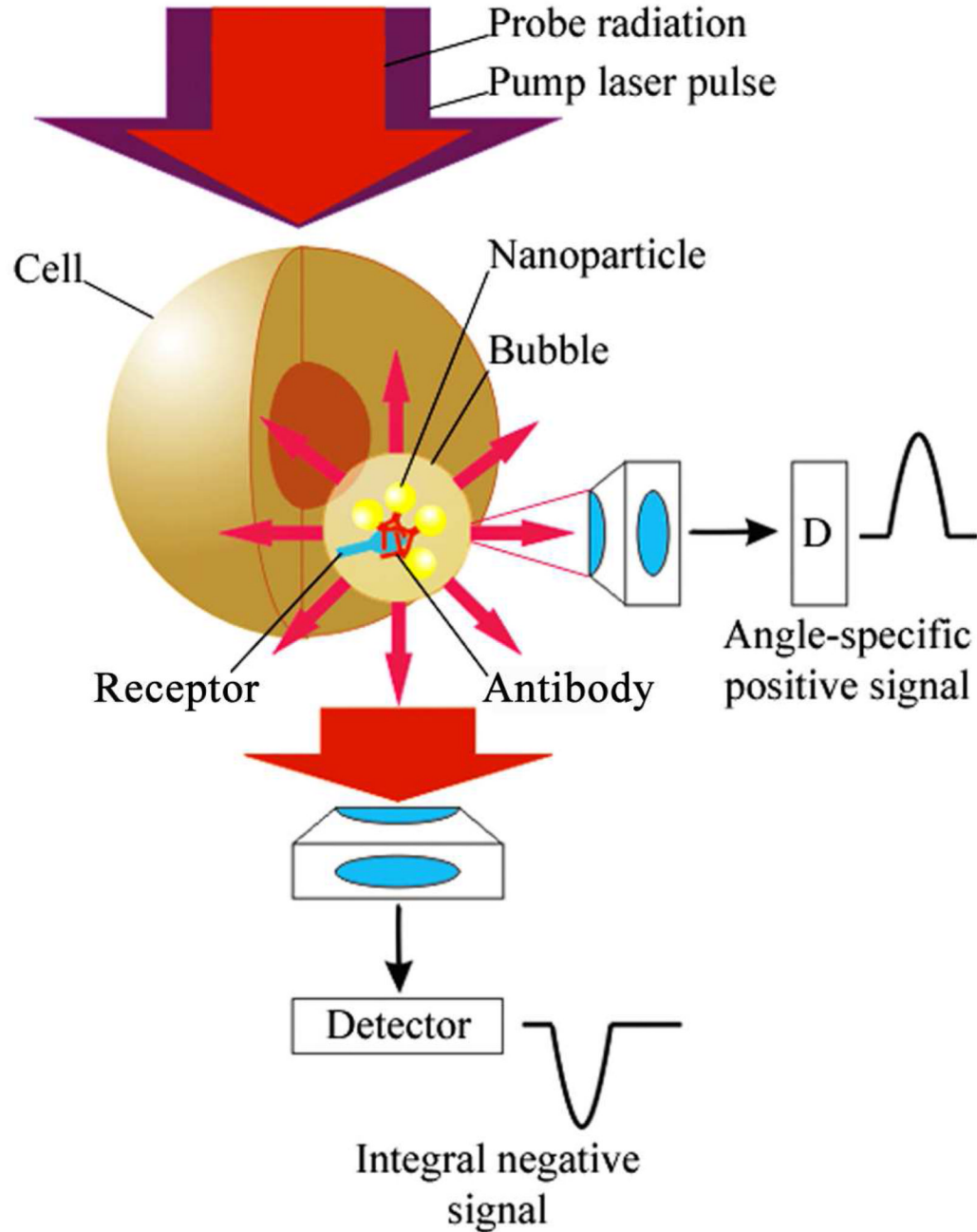
Figure 2.
Experimental scheme for optical generation and detection of plasmonic nanobubbles in cells *in vivo*: Gold NP conjugate with a cell-specific antibodies form the clusters during their endocytosis, the NP clusters generate the PNBs upon absorption of the pump laser pulse and scatter the probe laser radiation that is detected with a side or forward photodetectors.
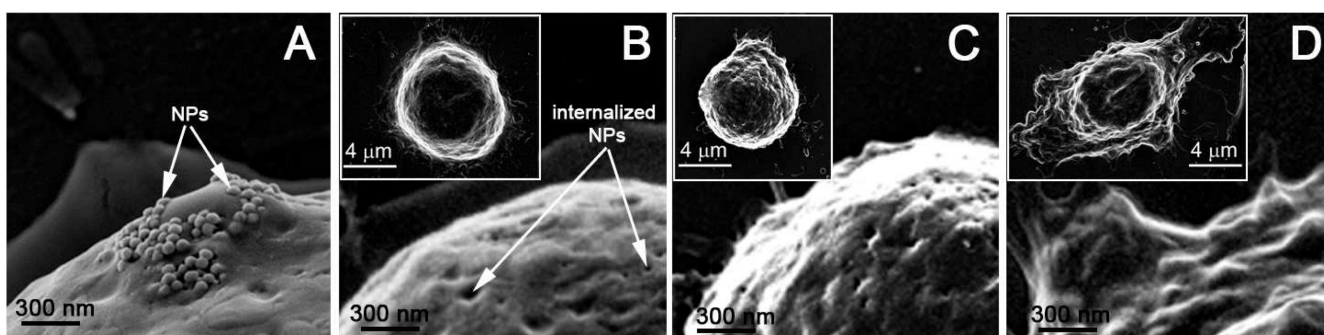
Figure 3.
Scanning electron microscopy images of cancer cells after the incubation with gold NPs show their membrane coupling (a) and internalization (b), and the result of the exposure to a single pump laser pulse that resulted in the non-invasive PNB with the lifetime of 25 ± 5 ns (c) and the ablative PNB with the lifetime of 300 ± 42 ns (d). The inserts show the images of the whole cells.
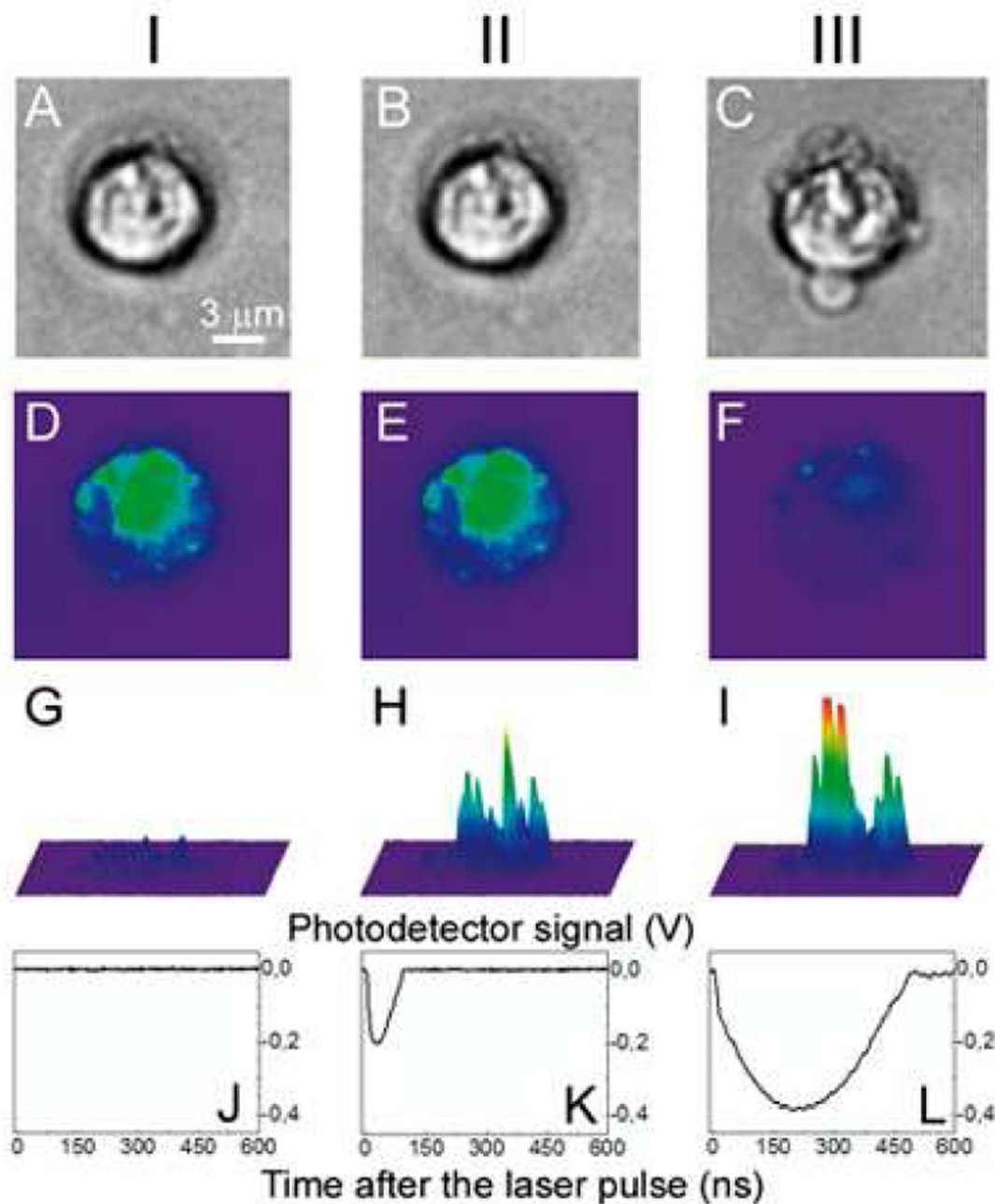
Figure 4.
Images of one prostate cancer cell incubated with gold NPs and DiI dye. I: before PNB, II: after the 1st PNB, III: after the 2nd PNB; (a–c): bright field images; (d–f): fluorescence of DiI ((d): before PNB, (e): after 1st PNB, (f): after 2nd PNB); (g–i): side scattering pulsed images of the cell (g), 1st PNB (h) and 2nd PNB (i); (j–l): corresponding time-responses obtained simultaneously with scattering images (g–i).

Figure 5.
Images of the zebrafish embryo with prostate cancer cells incubated with gold NPs and DiI dye: I: before PNB, II: after the 1st PNB, III: after the 2nd PNB; (a–c): bright field images; (d–f): fluorescence of DiI ((d): before PNB, (e): after 1st PNB, (f): after 2nd PNB); (g–i): side scattering pulsed images of the cell (g), 1st PNB (h) and 2nd PNB (i); (j–l): corresponding time-responses obtained simultaneously with scattering images (g–i). Cancer cell shown with an arrow.
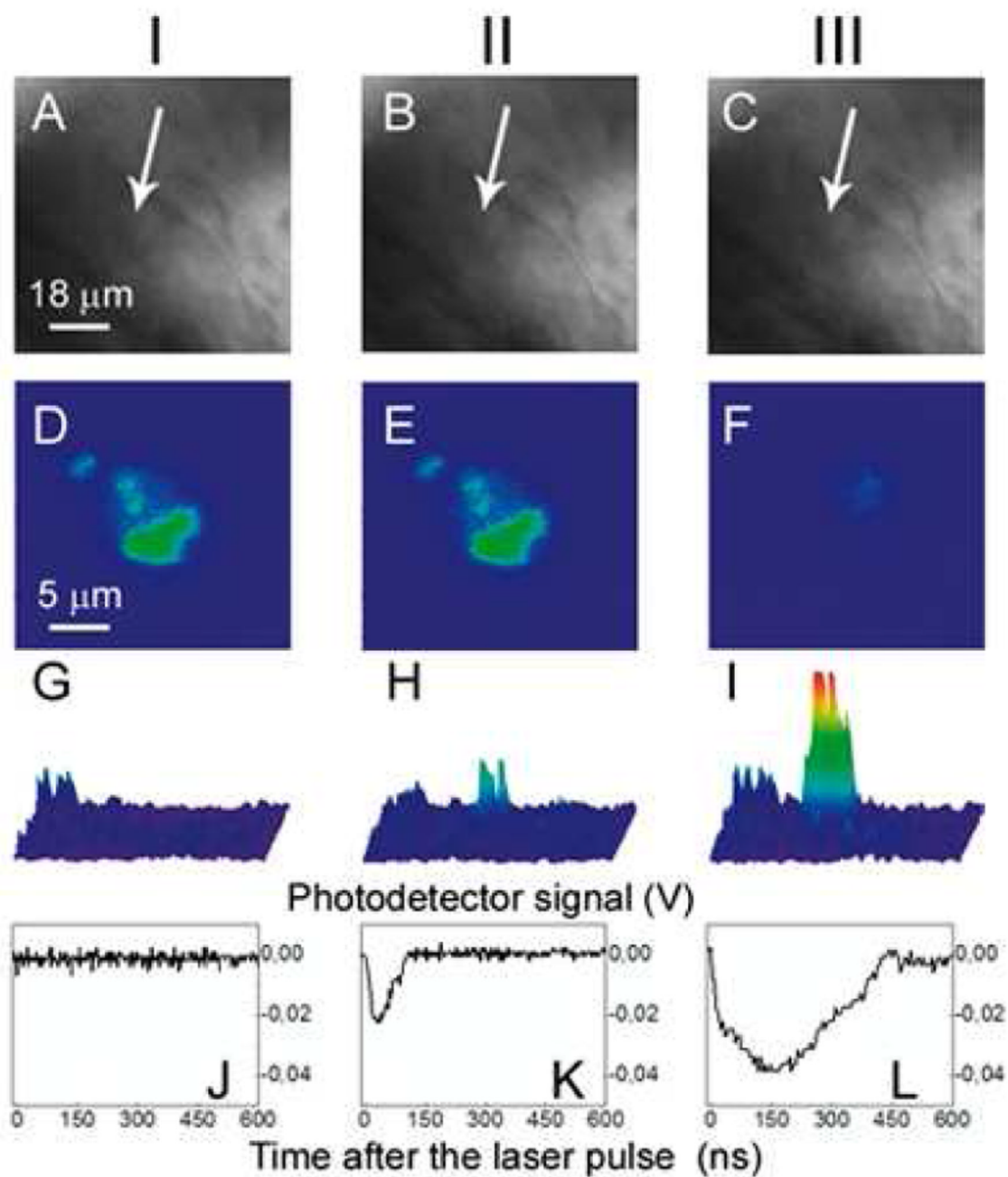
Table 1

Plasmonic nanobubbles parameters in three studied systems

Laser pulse fluence, mJ/cm²	PNB parameters	Zebrafish embryo			Cancer cells in vitro		Gold NPs in water	
		cells with NPs and DiI	cells with DiI	No cancer cells	NPs and DiI	DiI	NPs	NP clusters
	Generation threshold fluence, mJ/cm²	47	> 400	> 400	49	> 400	81	43
125 1st PNB	Probability, a.u.	1.0	0.0	0.0	1.0	0.04	0.95	1.0
	Lifetime, ns	62±17	0	0	72±15	0	45±10	93±30
	Optical contrast, a.u.	5.8±3	1	1	15±6	1	9±3	28±12
175 2nd PNB	Probability, a.u.	1.0	0.0	0.0	1.0	0.05	1.0	1.0
	Lifetime, ns	190±52	0	0	230±45	0	92±16	210±40
	Optical contrast, a.u.	19±8	1	1	49±23	1	27±7	130±30

Table 2

Potential medical applications of plasmonic nanobubbles

Application	PNB technology	Advantages
Flow cytometry and sorting	Flow cytometry, sorting and theranostics	Higher specificity and sensitivity; tunability of the probe; combination of cytometry and purification in one.
Gene transduction and cell therapy, delivery of drugs	Intracellular delivery of drugs, DNA	Selectivity and efficacy of cargo delivery (DNA, drugs) to specific cells; dynamic control of the release speed and efficacy; intracellular delivery.
Treatment of superficial cancers	Fiber optical theranostic system	Safety: cell selectivity in elimination of the tumor; combined diagnosis, treatment and guidance; sensitivity: early stage diagnosis/treatment.
Brachytherapy of deep tissue tumors	Fiber optical theranostic system	Safety and time (PNB instead of radiation); cell level selectivity of elimination of the tumor; combined diagnosis, treatment and guidance; sensitivity: early stage diagnosis/treatment.
Surgical guidance	Fiber optical system for monitoring surgical bed	Detection/elimination of residual tumor cells/tissues during surgical procedures; monitoring surgical tumor margins.